Full paper/Mémoire

# Amino-functionalized MIL-88B(Fe)-based porous carbon for enhanced adsorption toward ciprofloxacin pharmaceutical from aquatic solutions

Thuan Van Tran [a, b], Duyen Thi Cam Nguyen [a, b, c], Hanh Thi Ngoc Le [d], Dai-Viet N. Vo [a], Van-Dat Doan [e], Van-Phuc Dinh [f], Hong-Tham Thi Nguyen [a, b], Trinh Duy Nguyen [a, b, *], Long Giang Bach [b, g, **]

[a] Center of Excellence for Green Energy and Environmental Nanomaterials (CE@GrEEN), Nguyen Tat Thanh University, 300A Nguyen Tat Thanh, District 4, Ho Chi Minh City, 755414, Viet Nam
[b] NTT Hi-Tech Institute, Nguyen Tat Thanh University, 300A Nguyen Tat Thanh, District 4, Ho Chi Minh City, 755414, Viet Nam
[c] Department of Pharmacy, Nguyen Tat Thanh University, 298–300A Nguyen Tat Thanh, Ward 13, District 4, Ho Chi Minh City, 755414, Viet Nam
[d] Institute of Hygiene and Public Health, 159 Hung Phu, Ward 8, District 8, Ho Chi Minh City 700000, Viet Nam
[e] Faculty of Chemical Engineering, Industrial University of Ho Chi Minh City, 12 Nguyen Van Bao, Ward 4, Go Vap District, Ho Chi Minh City, 700000, Viet Nam
[f] Institute of Fundamental and Applied Sciences, Duy Tan University, 10C Tran Nhat Duat Street, District 1, Ho Chi Minh City, 700000, Viet Nam
[g] Center of Excellence for Functional Polymers and NanoEngineering, Nguyen Tat Thanh University, 300A Nguyen Tat Thanh, District 4, Ho Chi Minh City, 755414, Viet Nam

## ARTICLE INFO

## ABSTRACT

The present study focused on the synthesis of novel $NH_2$-PC700 adsorbent through the pyrolysis of $NH_2$-MIL-88B (Fe) material under different pyrolysis temperatures (500, 700, and 900 °C) and investigated its application for ciprofloxacin adsorption. The obtained adsorbents were characterized by X-ray powder diffraction (XRD), scanning electron microscopy (SEM), and nitrogen adsorption/desorption isotherm measurements. The parameters of the adsorption experiments that affect the removal efficiency, including solution pH (3−10), contact time (0−240 min), and initial concentration (10−40 mg/L), were also studied in detail. For the adsorption kinetic and isotherm studies, nonlinear models combined with error functions such as adjusted coefficient of determination ($R^2_{adj}$), mean relative error (MRE), and squares of the errors (SSE) were used to evaluate the compatibility between kinetic models (pseudo-first-order, pseudo-second-order, Elovich, and Bangham) and isotherm (Langmuir, Freundlich, Temkin, and Dubinin−Radushkevitch) adsorption equations. Besides, the role of amino functionalization for the ciprofloxacin (CFX) adsorption of $NH_2$-PC700 adsorbent was also explained. Through the Langmuir model, the maximum CFX adsorption capacity of $NH_2$-PC700 was calculated to be 102.5 mg/g, considerably higher than that of $NH_2$-MIL-88B (Fe). This outcome suggested that $NH_2$-PC700 could be a promising adsorbent for the CFX remediation.

© 2019 Académie des sciences. Published by Elsevier Masson SAS. All rights reserved.

* Corresponding author. Center of Excellence for Green Energy and Environmental Nanomaterials (CE@GrEEN), Nguyen Tat Thanh University, 300A Nguyen Tat Thanh, District 4, Ho Chi Minh City, 755414, Viet Nam.
** Corresponding author. NTT Hi-Tech Institute, Nguyen Tat Thanh University, 300A Nguyen Tat Thanh, District 4, Ho Chi Minh City, 755414, Viet Nam.
E-mail addresses: ndtrinh@ntt.edu.vn (T.D. Nguyen), blgiang@ntt.edu.vn (L.G. Bach).

## 1. Introduction

The extensive utilization of antibiotics for treatment of the bacteria-related diseases in humans and animals could accompany the release of the considerable amount of unmetabolized antibiotics and contaminant substances into the environment [1,2]. As a result, potential threats, including the development of antimicrobial resistance and adverse health effects associated with antibiotic contamination, have been well identified and increasingly reported [3]. For example, M.J. Ahmed and B.H. Hameed found a robust correlation between the development of antimicrobial resistance and the occurrence of antibiotics in aquatic systems [4]. Danner et al. also explained that residues of antibiotics in hospital effluents or water sources stemming from pharmaceutical manufacturers could contain many kinds of antibiotics; without any pretreatments, they are likely to enter the food chains, in turn causing adverse impacts on human health [5]. As a consequence, treatment techniques for antibiotics in wastewater have been receiving great attention. Among treatment methods, adsorption has been regarded as a simple, sustainable, and efficient approach [6].

Several sorbent materials, such as carbon-based materials, mesoporous clay materials, zeolites, and biosorbents, have been developed to remove antibiotics from water [7,8]. In particular, porous carbon derived from metal-organic frameworks (MOFs), crystalline material under the combination of metal ions and organic linkers [9], has been applied as a promising adsorbent, showing superior features in comparison with traditional ones (e.g., activated carbon) [8]. Indeed, Ahmed et al. [10] fabricated a series of MOF-derived carbons by the pyrolysis of zeolite imidazole framework (ZIF-8) and metal azolate framework-6 (MAF-6) [11], which exhibited a high adsorption efficiency for eliminating a wide range of pharmaceuticals such as salicylic acid, clofibric acid, diclofenac sodium, and sulfamethoxazole [12,13].

Moreover, MOFs (MIL-101) were surface-modified with enriching of nitrogen groups such as protonated polyaniline, resulting in the (pANI)@MIL-101 with outstanding adsorption capacities ($Q_o$) for removal of quinoline ($Q_o$ = 556 mg/g) and neutral indole from *n*-octane ($Q_o$ = 602 mg/g) [14]. Another work also demonstrated the role of modifying the structure of porous carbon by doping nitrogen-containing functional groups to remove the personal care products (PCPs) efficiently [11]. Bhadra et al. [8] discussed the MOF-derived carbonaceous materials enriched with nitrogen by the direct carbonization method of MOFs prepared from N-containing linkers for many applications in adsorption and catalysis.

In our previous studies, such porous carbons, synthesized from MIL-53 (Fe), have been used as an effective adsorbent to treat the ciprofloxacin (CFX) in aqueous media, resulting in a high adsorption capacity (90.9 mg/g), good reusability (up to five cycles), and chemical stability [15]. The present study continued to develop another novel adsorbent derived from amino-functionalized MIL-88B (Fe) as nitrogen-doping porous carbons, enabling a new and promising approach for CFX remediation. To our best knowledge, the structural characterization and adsorption performance for removing CFX using these NH$_2$-MIL-88B (Fe)–derived carbon adsorbents have not been reported previously; therefore, more relevant studies are necessary.

## 2. Experimental section

### 2.1. Chemicals and analytical instruments

All chemicals, including CFX, 2–aminoterephthalic acid (NH$_2$–BDC), and iron chloride FeCl$_3$·6H$_2$O, were purchased from Sigma-Aldrich. The D8 Advance Bruker powder diffractometer was used to record the X-ray powder diffraction (XRD, Hitachi Inc., Krefeld, Germany) profiles using Cu K$\alpha$ beams as excitation sources. The S4800 instrument (JEOL, Tokyo, Japan) was implemented to capture the scanning electron microscopy (SEM) images with the magnification of 7000 using an accelerating voltage source (15 kV). The N$_2$ adsorption/desorption isotherm and pore size distribution data were recorded on the Micromeritics 2020 volumetric adsorption analyzer system (Micromeritics Inc., Norcross, GA, USA). A UV-vis spectrophotometer (Shimadzu, Kyoto, Japan) was used to determine CFX concentrations at 278 nm.

### 2.2. Synthesis procedure for NH$_2$–MIL-88B(Fe) and NH$_2$-PCx materials

The MOF NH$_2$–MIL-88B(Fe) was prepared by the microwave-assisted solvothermal method as described in the previous literature [16]. In a typical synthesis procedure, a homogeneous mixture of 2.3 mmol of NH$_2$–BDC (0.417 g) and 0.23 mmol of FeCl$_3$·6H$_2$O (0.622 g) in 50 mL of dimethylformamide (DMF) was kept in an ultrasonic bath with continuous shaking for 10 min to remove air bubbles and then transferred into a microwave vial. The mixture was heated to 150 °C under microwave irradiation (200 W) for 10 min. The product was taken out of the microwave oven, washed with DMF (3 × 10 mL) and chloroform (3 × 10 mL) and then dried under vacuum. The NH$_2$-MIL-88B(Fe)–derived porous carbons were formed by applying the carbonization strategy [17]. In detail, as-synthesized NH$_2$-MIL-88B(Fe) was pyrolyzed at *x* °C (*x* represents 500, 700, and 900 °C) under N$_2$ nitrogen (2 °C per min, 400 cm$^3$ N$_2$ per min) for 4 h. The black powders (NH$_2$-PC*x*) were collected, washed with dilute HCl, and stored carefully. Scheme 1 illustrates the synthesis strategy of NH$_2$-MIL-88B (Fe) and NH$_2$-PC*x* materials.

### 2.3. Experimental batches

The present study used experimental data from each separate run to investigate the adsorption properties of CFX in aqueous solutions. Each beaker containing (NH$_2$-MIL and NH$_2$-PC*x*) adsorbents (5.0 mg) and 50 mL of CFX solution at various concentrations (10–40 mg/L) was shaken at 200 rpm and at room temperature. Investigation with regard to the effect of pH was conducted under adjusting the acidity and basicity of CFX solution (in the range from 3 to 10). To examine the effect of contact time,
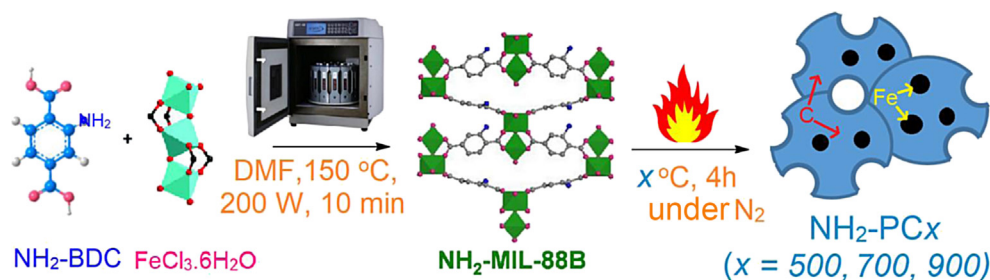
**Scheme 1.** Synthesis route of NH$_2$-MIL-88B (Fe) and its pyrolysis products (NH$_2$-PC$x$). The structure of NH$_2$-MIL-88B and iron (III) clusters was reproduced from the study by Liédana et al. [18].

the CFX concentrations at various regular periods (0, 10, 30, 60, 90, 120, 150, 180, and 240 min) were determined. Finally, various concentrations (10–40 mg/L) were selected for performing the adsorption process reaching an equilibrium state. Key formulae to identify the removal $Y$ (%) and adsorption capacity $Q$ (mg/g) are listed in the following (Eqs. 1 and 2, respectively). Note that $C_o$, and $C_e$ are defined as initial and equilibrium CFX concentrations (mg/L), respectively; $m$ (g) and $V$ (ml) are the mass of adsorbent and volume of solution, respectively. To assess the compatibility of kinetic and isotherm models, we used three error functions including adjusted coefficient of determination $(R_{adj})^2$, mean relative error (MRE), and squares of the errors (SSE), which were defined in the previous study [19].

$$Y = \frac{C_o - C_e}{C_o} \cdot 100 \qquad (1)$$

$$Q = \frac{C_o - C_e}{m} \cdot V \qquad (2)$$

### 2.4. Adsorption kinetics

Adsorption kinetics are used to find out the relationship between contact time $t$ (min) and kinetic adsorption capacity (mg/g) via fitting of kinetic adsorption data with different forms of nonlinear kinetic models. We applied four common models, including pseudo-first-order, pseudo-second-order, Elovich, and Bangham models. Table 1 listed the mathematical forms for these models together with their parameters [20].

### 2.5. Adsorption isotherms

Adsorption isotherms are used to find out the relationship between equilibrium concentration $C_e$ (mg/g) and equilibrium adsorption capacity (mg/g). Similar to kinetics adsorption, various nonlinear isotherm models were estimated with respect to isotherm adsorption data. We applied four standard models, including Freundlich, Langmuir, Temkin, and Dubinin–Radushkevitch (D–R) models. Table 2 also listed the mathematical forms together with their parameters [21].

**Table 1**
A description of nonlinear kinetic equations.

| Kinetics | Equation | Eq. no. | Parameters | Unit |
|---|---|---|---|---|
| Pseudo-first-order | $Q_t = Q_1 \cdot (1 - \exp(-k_1 t))$ | (3) | $k_1$ $Q_1$ | min$^{-1}$ mg/g |
| Pseudo-second-order | $Q_t = \dfrac{t}{\frac{1}{k_2 Q_2^2} + \frac{t}{Q_2}}$ | (4) | $k_2$ $Q_2$ $H = k_2(Q_2)^2$ | g/mg min mg/g |
| Elovich | $Q_t = \dfrac{1}{\beta} \ln(1 + \alpha\beta t)$ | (5) | $\alpha$ $\beta$ | mg/g min g/mg |
| Bangham | $Q_t = k_B \cdot t^{\alpha_B}$ | (6) | $k_B$ $\alpha_B$ | mL/(g/L) |

### 3. Results and discussion

#### 3.1. Structural characterization

The materials involving NH$_2$-MIL-88B (Fe) and NH$_2$-PC700 were first analyzed by the XRD technique, as shown in Fig. 1. It is evident that the diffraction profile of NH$_2$-MIL-88B (Fe) was completely different from that of NH$_2$-PC700. Indeed, according to Fig. 1(a), the diffraction patterns of the as-synthesized NH$_2$-MIL-88B (Fe) have many emergent peaks at 6.6° (100), 8.6° (101), 9.2° (002), 12.4° (102), 16.2° (200), 16.8° (103), 17.8° (202), 20.0° (210), 22.0° (212), 24.8° (300), and 27.0° (311), suggesting that this MOF obtained a highly crystalline structure [16]. The XRD profile of the as-synthesized NH$_2$-MIL-88B (Fe)

**Table 2**
A description of nonlinear isotherm equations.

| Isotherms | Equation | Eq. no. | Parameters | Unit |
|---|---|---|---|---|
| Freundlich | $Q_e = K_F C_e^{1/n}$ | (7) | $k_F$ $1/n$ | (mg/g)/(mg/L)$^{1/n}$ |
| Langmuir | $Q_e = \dfrac{Q_m K_L C_e}{1 + K_L C_e}$ | (8) | $k_L$ $Q_m$ $R_L = 1/(1 + R_L C_o)$ | L/mg mg/g |
| Temkin | $Q_e = B_T \ln(k_T C_e)$ | (9) | $k_T$ $B_T$ | L/mg |
| D–R | $Q_e = Q_m \exp(-B\varepsilon^2)$ | (10) | $Q_m$ $B$ | mg/g |

D–R, Dubinin–Radushkevitch.

was highly in line with those reported by several previous works, indicating that NH$_2$-MIL-88B (Fe) precursor was successfully fabricated by the microwave-assisted solvothermal method [16,22–24]. As seen in Fig. 1(b), the XRD profile of NH$_2$-PC700 gave several typical peaks. In detail, the existence of zero-valent iron (Fe: JCPDS No. 65–4899) in its structure can be proved by the presence of peaks at around 44.8° and 65.2°, while a broad peak from 20° to 30° was attributable to the graphitic structure of porous carbon, which was formed by the decomposition of NH$_2$-MIL-88B (Fe) [25–27].

To further characterize the structure of NH$_2$-MIL-88B (Fe) and NH$_2$-PC700, the N$_2$ adsorption/desorption isotherm measurement could be conducted. According to Fig. 2(a), the isotherm curve of NH$_2$-PC700 showed an obvious hysteresis loop with the pattern similar to type IV, and there was an adsorption isotherm line at shallow relative pressure, thus implying that this material could be suggested to have both microporous and mesoporous structures [28,29]. Meanwhile, the figure for NH$_2$-MIL-88B (Fe) demonstrated a mainly nonporous or macroporous structure (type III) [30]. The measured surface area and pore volume of two materials also indicate the same trend, respectively, reaching 215.1 m$^2$/g and 0.2 cm$^3$/g for NH$_2$-PC700 and 5.9 m$^2$/g and 0.035 cm$^3$/g for NH$_2$-MIL-88B. Fig. 2(b) illustrated the pore size distribution plots of mentioned materials. The NH$_2$-PC700 contains pores of different size ranges including micropores (<2 nm), mesopores (2–50 nm), and macropores (>50 nm), while the pore size of NH$_2$-MIL-88B is distributed in the size range of greater than 50 nm, which is indicative of a nonporous structure [31].

The morphological properties of NH$_2$-MIL-88B (Fe) and NH$_2$-PC700 were investigated by SEM. Figs. 3(a–c) show that the synthesized NH$_2$-MIL-88B(Fe) seems to have heterogeneous crystals. The larger crystals display a needle-shaped morphology, and the smaller particles display a typical octahedral morphology [32]. Figs. 3(d–f) indicate that the NH$_2$-PC700 has a highly amorphous and defective surface. Besides, the point of zero charge (pH$_{pzc}$) of NH$_2$-PC700 was determined at 6.0. With this value of pH$_{pzc}$, it is understandable that the surface of the adsorbent tends to be charged positively at pH < 6.0 and, in contrast, charged negatively at pH > 6.0 [33]. These characteristics of NH$_2$-PC700 may shed light on its adsorption toward CFX molecules.

To gain insight into the existence of nitrogen of amino groups in NH$_2$-PC700, the use of another more accurate technique is necessary. Fig. 4 compares the X-ray photoelectron spectroscopy (XPS) survey spectra of NH$_2$-MIL-88B and NH$_2$-PC700. At the first glance, both these adsorbents contain four main elements which are carbon (C 1s), nitrogen (N 1s), oxygen (O 1s), and iron (Fe 2p). In particular, Fig. 4 (b) could confirm the existence of both nitrogen and oxygen in the structure of NH$_2$-PC700 although a decrease in their intensity between NH$_2$-MIL-88B and NH$_2$-PC700 may be observed. In contrast, the intensity of carbon seems to become larger, which may be attributable to the effect of pyrolysis at 700 °C. While this process may mostly break the structure of NH$_2$-MIL-88B and transform its linkers into carbon skeletons, amino groups and oxygen-rich groups were still maintained, permitting the adsorbent to uphold its adsorptivity [11].

## 3.2. Adsorption study

### 3.2.1. Effect of the pyrolysis temperature

The effect of pyrolysis temperature (500–900 °C) on CFX adsorption capacity is shown in Fig. 5(a). It is evident that changes in pyrolysis temperature of NH$_2$-MIL-88B (Fe) could result in altered adsorption capacity. Indeed, the NH$_2$-MIL-88B (Fe) precursor only adsorbed 6.0 mg of CFX antibiotic per gram of adsorbent, but its pyrolysis products showed considerably higher adsorption capacities. Among them, NH$_2$-PC700 formed by the pyrolysis of the precursor at 700 °C obtained the highest capacity value ($Q = 28.0$ mg/g). Therefore, we used NH$_2$-PC700 as an adsorbent for subsequent investigations.

### 3.2.2. Effect of the pH of the solution

The adsorption efficiency of CFX onto NH$_2$-PC700 was investigated at different pH values (3–10). According to Fig. 5(b), the CFX adsorption capacity in the acidic solution (e.g., pH 3) was unconducive. As the pH increased, the adsorbability improved, and the adsorption ability of NH$_2$-PC700 reached the peak (28.0 mg/g) at an optimum pH of 6.
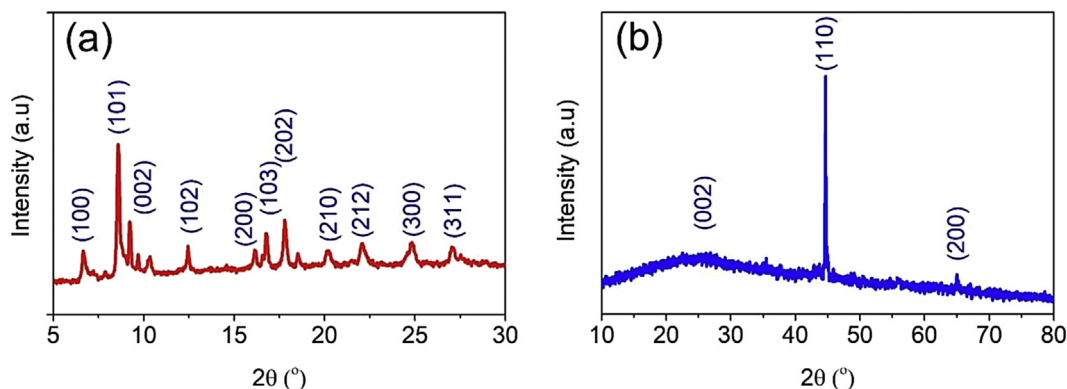


**Fig. 1.** XRD diffraction patterns of NH$_2$-MIL-88B (Fe) (a) and NH$_2$-PC700 (b) materials. XRD, X-ray powder diffraction.
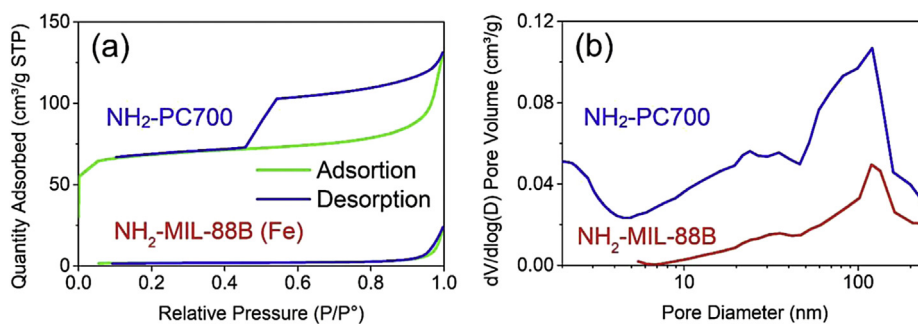
**Fig. 2.** Nitrogen adsorption/desorption isotherms (a) and pore size distribution plots (b) of NH$_2$-MIL-88B (Fe) and NH$_2$-PC700 materials.
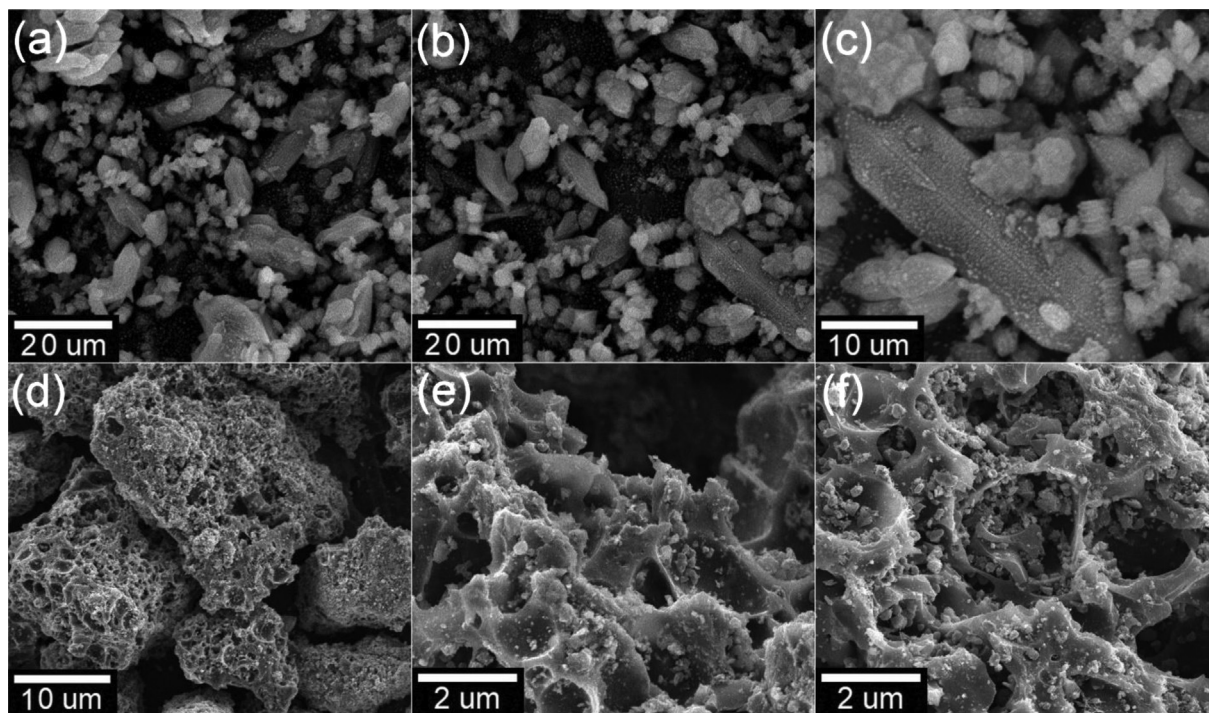


**Fig. 3.** SEM images of NH$_2$-MIL-88B (Fe) (a–c) and NH$_2$-PC700 (d–f) materials. SEM, scanning electron microscopy.
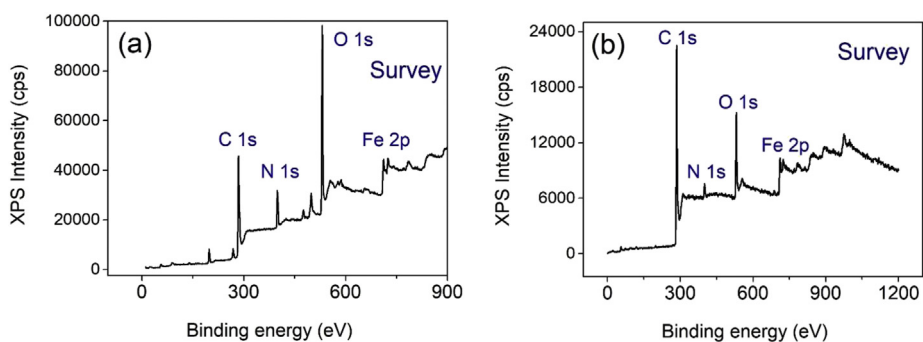


**Fig. 4.** XPS survey spectra of NH$_2$-MIL-88B (a) and NH$_2$-PC700 (b). XPS, X-ray photoelectron spectroscopy.
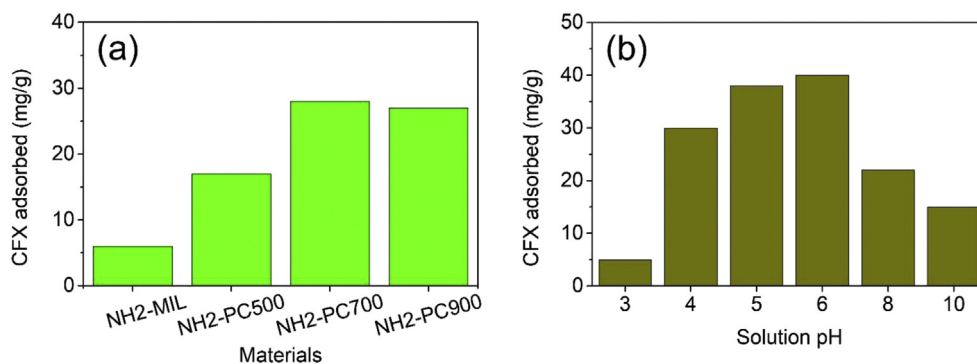
**Fig. 5.** Effect of pyrolysis temperature (a) and solution pH (b) on CFX adsorption capacity. CFX, ciprofloxacin.

This result was commensurate with previous reports [34,35]. In contrast, this process becomes inappropriate in basic solutions (pH $\geq$ 8).

As mentioned, the point of zero charge ($pH_{pzc}$) of $NH_2$-PC700 was 6.0, and CFX molecules have two pKa points (5.9 and 8.9) [36]. At pH > 8.9, the adsorption was hampered because of the existence of electrostatic repulsion between the negatively charged surfaces of $NH_2$-PC700 and anions $CFX^{2-}$. At pH 6, it was demonstrated that CFX could be in a mixture of zwitterionic and cationic forms, possibly causing several interactions (e.g., H-bond, $\pi-\pi$ interaction, and electrostatic attraction) and in turn leading to enhanced adsorption capacity [37]. At a very low value, the $CFXH_2^{2+}$ cations become predominant, resulting in electrostatic repulsion between the positively charged surfaces of $NH_2$-PC700 and cations of CFX, and therefore, the adsorption becomes difficult [38].

### 3.2.3. Effect of contact time

Generally, for the optimization purpose in industrial applications, any adsorption processes achieving a short completion time could bring more advantages in effectiveness and efficiency; therefore, the contact time plays a crucial role in adsorption investigation. Fig. 6(a) displays the effect of equilibrium time on CFX adsorption efficiency for four concentrations (10–40 mg/L). These adsorption curves seem to be smooth and progressive, and there is no abnormality in adsorption capacity at each period. These trends provide the proofs of forming a type of monolayer

coverage toward CFX molecules relying on the surface of $NH_2$-PC700 [39]. In addition, CFX molecules rapidly adsorbed on the $NH_2$-PC700 surface during the first 60-min period, and then, this process became more saturated and reached equilibrium within 240 min for all concentrations. As a result, the shaking period during the 240 min could be selected as an optimum value of contact time.

### 3.2.4. Effect of initial concentration

To survey the effect of initial CFX concentration on adsorption capacity of $NH_2$-PC700, we selected the range of concentration from 10 mg/L to 40 mg/L, the amount of adsorbent at 0.1 g/L, and the contact time at 240 min. The equilibrium adsorption capacity ($Q_e$) can be identified based on the residual concentration ($C_e$) by UV-vis spectroscopy. The curve describing the relationship between $C_e$ and $Q_e$ is shown in Fig. 5(b). The graph of $C_e$ versus $Q_e$ in Fig. 6(b) demonstrates that the increase of initial CFX concentration can result in a considerable enhancement of adsorption capacity. However, a positive relationship was nonlinear. Indeed, the $Q_e$ values have been improved from 40 mg/g to 80 mg/g as the concentration rose from 10 mg/L to 40 mg/L. Hameed and Rahman [39] explained that there are three consecutive steps (adsorbate migration from solution, their movement from the surface to pore of adsorbent, and adsorption on active sites) of mass transport influencing the adsorption of solute in solution. Therefore, it is suggested that the adsorption of CFX at higher concentration requires a longer time to reach the saturation.
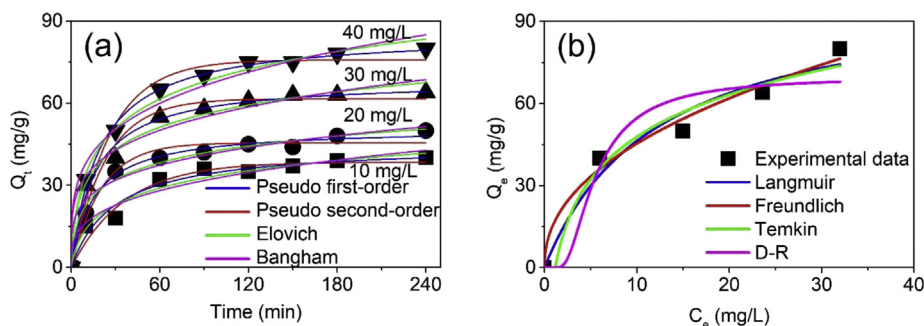


**Fig. 6.** Effect of contact time (a) at different concentrations (10–40 mg/L) and (b) equilibrium concentration (b) on CFX adsorption capacity onto $NH_2$-PC700. CFX, ciprofloxacin; D–R, Dubinin–Radushkevitch.

**Table 3**
Kinetic constants for the adsorption of CFX over $NH_2$-PC700 material.

| Kinetic models | Equation | Parameters | CFX concentrations | | | |
|---|---|---|---|---|---|---|
| | | | 10 mg/L | 20 mg/L | 30 mg/L | 40 mg/L |
| Pseudo-first-order | $Q_t = Q_1 \cdot (1 - \exp(-k_1 t))$ | $k_1$ ($min^{-1}/(mg/L)^{1/n}$) | 0.0276 | 0.0493 | 0.0436 | 0.0390 |
| | | $Q_1$ (mg/g) | 38.5 | 45.5 | 61.6 | 75.8 |
| | | MRE (%) | 9.67 | 5.65 | 7.07 | 5.95 |
| | | SSE | 55.59 | 52.73 | 112.40 | 109.65 |
| | | $(R_{adj})^2$ | 0.9584 | 0.9712 | 0.9654 | 0.9782 |
| Pseudo-second-order | $Q_t = \dfrac{t}{\dfrac{1}{k_2 Q_2^2} + \dfrac{t}{Q_2}}$   $H = k_2 \cdot Q_2^2$ | $k_2 \cdot 10^4$ (g/(mg.min)) | 7.67 | 12.80 | 9.21 | 6.16 |
| | | $Q_2$ (mg/g) | 44.9 | 50.9 | 68.5 | 85.6 |
| | | $H$ | 1.55 | 3.32 | 4.32 | 4.51 |
| | | MRE (%) | 8.40 | 2.63 | 3.58 | 2.24 |
| | | SSE | 44.51 | 14.87 | 37.61 | 15.38 |
| | | $(R_{adj})^2$ | 0.9667 | 0.9919 | 0.9884 | 0.9970 |
| Elovich | $Q_t = \dfrac{1}{\beta} \ln(1 + \alpha \beta t)$ | $\alpha$ [mg/(g.min)] | 3.24 | 10.49 | 14.57 | 12.20 |
| | | $\beta$ (g/mg) | 0.11 | 0.11 | 0.08 | 0.06 |
| | | MRE (%) | 7.31 | 4.36 | 4.06 | 3.46 |
| | | SSE | 48.10 | 25.35 | 46.44 | 43.39 |
| | | $(R_{adj})^2$ | 0.9640 | 0.9861 | 0.9857 | 0.9914 |
| Bangham | $Q_t = k_B \cdot t^{\alpha_B}$ | $k_B$ [mL/(g/L)] | 8.09 | 14.57 | 19.48 | 21.40 |
| | | $\alpha_B$ | 0.30 | 0.23 | 0.23 | 0.25 |
| | | MRE (%) | 8.45 | 6.51 | 5.97 | 5.76 |
| | | SSE | 65.48 | 48.18 | 82.98 | 116.23 |
| | | $(R_{adj})^2$ | 0.9510 | 0.9737 | 0.9745 | 0.9769 |

CFX, ciprofloxacin; MRE, mean relative error; SSE, squares of the errors.

### 3.2.5. Adsorption kinetics

Herein, nonlinear adsorption kinetics, including pseudo-first-order, pseudo-second-order, Elovich, and Bangham models, were applied. Table 3 lists the values of parameters together with their errors. We used the coefficient of determination (adjusted $R^2$) along with two error functions involving MRE and SSE to assess the compatibility between models. By comparing the magnitudes of these error functions, the most appropriate models could be justified for adsorption kinetics [40]. Theoretically, a model with lower error and higher correlation shows better compatibility and confidence levels [41–43].

In general, all nonlinear models well predicted experimental data because their respective coefficients of the determination reached closely 1.0. The pseudo-second-order models achieved the highest coefficients of determination (0.9667–0.9970) and the lowest errors (MRE = 2.24–8.40 %, SSE = 14.87–44.51), except for a case of CFX adsorption model at concentration 10 mg/L where a higher value of MRE was recognized in the pseudo-second-order model. However, its SSE was lower and the adjusted $R^2$ was higher than in other models, suggesting that the adsorption kinetics still obeyed the pseudo-second-order kinetics. These results suggested the high compatibility

**Table 4**
Isotherm constants for the CFX adsorption over $NH_2$-PC700 material.

| Kinetic models | Equation | Parameters | Value |
|---|---|---|---|
| Langmuir | $Q_e = \dfrac{Q_m K_L C_e}{1 + K_L C_e}$   $R_L = \dfrac{1}{1 + K_L C_o}$ | $k_L$ (L/mg) | 0.08 |
| | | $Q_m$ (mg/g) | 102.50 |
| | | $R_L$ | 0.23 |
| | | MRE (%) | 10.35 |
| | | SSE | 127.40 |
| | | $(R_{adj})^2$ | 0.9534 |
| Freundlich | $Q_e = K_F C_e^{1/n}$ | $k_F$ $(mg/g)/(mg/L)^{1/n}$ | 16.18 |
| | | $1/n$ | 0.45 |
| | | MRE (%) | 6.81 |
| | | SSE | 54.75 |
| | | $(R_{adj})^2$ | 0.9800 |
| Tempkin | $Q_e = B_T \ln(k_T C_e)$   $B_T = \dfrac{RT}{b}$ | $B_T$ | 22.37 |
| | | $k_T$ (L/mg) | 0.85 |
| | | MRE (%) | 8.81 |
| | | SSE | 107.60 |
| | | $(R_{adj})^2$ | 0.9804 |
| D–R | $Q_e = Q_m \exp(-B\varepsilon^2)$   $\varepsilon = RT \ln\left(1 + \dfrac{1}{C_e}\right)$   $E = \dfrac{1}{\sqrt{2B}}$ | $B$ ($kJ^2/mol^2$) | 4.35 |
| | | $Q_m$ (mg/g) | 69.65 |
| | | $E$ (kJ/mol) | 0.34 |
| | | MRE (%) | 12.85 |
| | | SSE | 313.68 |
| | | $(R_{adj})^2$ | 0.8853 |

CFX, ciprofloxacin; MRE, mean relative error; SSE, squares of the errors.

**Table 5**
The comparative CFX adsorption efficiency of nanomaterial adsorbents.

| No. | Adsorbents | Maximum adsorption capacity (mg/g) | Ref. |
|---|---|---|---|
| 1 | $NH_2$–PC700 | 102.5 | (*) This work |
| 2 | MPC800 | 90.9 | [15] |
| 3 | MIL-53 (Fe) | 42.7 | [15] |
| 4 | Bamboo charcoal | 36.2 | [47] |
| 5 | MIL-101/$Fe_3O_4$ | 63.3 | [48] |
| 6 | $Fe_3O_4$/C | 90.1 | [45] |
| 7 | Magnetic mesoporous carbon composite | 98.3 | [49] |
| 8 | $Fe_3O_4$/C | 74.7 | [49] |
| 9 | Dioctahedral clay minerals | 13.1 | [50] |
| 10 | Fe-doped MCM-41 | 83.3 | [51] |
| 11 | $Fe_3O_4$/AC/chitosan | 90.1 | [52] |

CFX, ciprofloxacin.

and more predominance of the pseudo-second-order model with the overall adsorption rate via chemisorption [44]. The present outcomes were highly commensurate with our previous study and other studies, where characteristics of adsorption kinetics for CFX were reported [15,44,45].

### 3.2.6. Adsorption isotherms

Primarily, adsorption isotherm can be used to describe how well CFX molecules interact with the surface of $NH_2$-PC700. To find out the relationship between the amount of CFX antibiotic adsorbed and its equilibrium concentration, we fitted the experimental data with several standard isotherms including Langmuir, Freundlich, Temkin, and D−R isotherm models. Parameters calculated from nonlinear isotherms are summarized in Table 4.

Among the isotherm models, both Freundlich and Temkin isotherms had almost equivalent values of adjusted $R^2$ (0.9800 and 0.9894, respectively). However, the Freundlich model was more well fitted with experimental data because this equation acquired the lower error functions (MRE = 6.81% and SSE = 54.75) than the Temkin model (MRE = 8.81% and SSE = 107.60). Therefore, the adsorption isotherm can be explained by the Freundlich model, which assumes that the adsorption obeyed a multilayer behavior [44]. In addition, the adsorption of CFX onto $NH_2$-PC700 was a favorable process because the $R_L$ and 1/n obtained from the respective Langmuir and Freundlich equations were less than 1.0 [46]. In particular, the maximum adsorption capacity calculated from the Langmuir model was found to be 102.5 mg/g and higher than that obtained from previous studies (Table 5), suggesting that $NH_2$-PC700 can be an outstanding candidate to remove the CFX from wastewater.

### 3.3. Role of amino functionalization

In our previous study, the porous carbon synthesized from MIL-53 (Fe) at 800 °C exhibited the maximum CFX adsorption capacity of 90.9 mg/g. Herein, we used the same template, but it was modified with amino (-$NH_2$) groups based on 2-aminoterephthalic acid as a linker via the direct carbonization of MOFs prepared from these N-containing linkers. The amino-functionalized porous carbon gave a higher adsorption capacity of 102.5 mg/g. The improved adsorption of CFX antibiotic could be attributable to the amino (-$NH_2$) groups.

Chemically, amino groups possess electron-rich nitrogen, presenting a relatively strong Lewis base. Meanwhile, CFX molecules were fluorinated and constituted by amino, tertiary amine, and carboxylic (-COOH) groups. Therefore, the presence of amino groups on the surface of porous carbon can bridge some interactions (e.g., H-bond) with amino, tertiary amine, and carboxylic groups of CFX. Together with other principal interactions (van der Waals, hydrophobic, and $\pi - \pi$ interaction), the adsorption can be improved [53]. Bhadra et al. [8] also asserted the role of basic groups originated from the N-containing linkers in the adsorption of the antibiotic. This hypothesis was evidenced by the better performance of N-doped porous carbon toward nitrogen-containing compounds (e.g., indole and quinoline) and sulfur-containing compounds (e.g., benzothiophene and dibenzothiophene) in comparison with the cases of N-free porous carbons [10,14,54]. Based on the aforementioned findings, we argue that the porous carbon from N-containing MOFs may rely mostly on the N species to create more H-bonding interaction, showing higher adsorption efficiency [55]. By this way, the amino functionalization can become an efficient approach for the liquid-phase adsorption to purify water and fuel.

### 4. Conclusion

The novel $NH_2$-PC700 has been successfully synthesized from the precursor $NH_2$-MIL-53 (Fe). The characterization results revealed that $NH_2$-PC700 had a porous and defective structure together with a high surface area (215.1 $m^2$/g). For adsorption experiments, the effect of pyrolysis

temperature, solution pH, contact time, and initial concentration was systematically investigated. The adsorption results demonstrated that 700 °C and pH of 6 were the optimum pyrolysis temperature and solution pH values, respectively. Nonlinear kinetic data asserted that the adsorption adhered to the pseudo-second-order model and chemisorption was an effective adsorption mechanism, while nonlinear isotherm obeyed the Freundlich isotherm via multilayer behavior. Compared with the maximum CFX adsorption capacity reported by previous works, this study showed better adsorption results (up to 102.5 mg/g).

## Acknowledgements

## References

[1] D. Jasovský, J. Littmann, A. Zorzet, O. Cars, Upsala J. Med. Sci. 121 (2016) 159–164.
[2] M. Lekshmi, P. Ammini, S. Kumar, M.F. Varela, Microorganisms 5 (2017).
[3] I. Roca, M. Akova, F. Baquero, J. Carlet, M. Cavaleri, S. Coenen, J. Cohen, D. Findlay, I. Gyssens, O.E. Heure, New Microbes New Infect 6 (2015) 22–29.
[4] M.J. Ahmed, B.H. Hameed, Ecotoxicol. Environ. Saf. 149 (2018) 257–266.
[5] M.C. Danner, A. Robertson, V. Behrends, J. Reiss, Sci. Total Environ. 664 (2019) 793–804.
[6] A.M. Aljeboree, A.N. Alshirifi, J. Pharm. Sci. Res. 10 (2018) 2252–2257.
[7] J. Akhtar, N.A.S. Amin, K. Shahzad, Desalin. Water Treat. 57 (2016) 12842–12860.
[8] B.N. Bhadra, A. Vinu, C. Serre, S.H. Jhung, Mater. Today 25 (2018) 88–111.
[9] T. V Tran, H.T.N. Le, H.Q. Ha, X.N.T. Duong, L.H.-T. Nguyen, T.L.H. Doan, H.L. Nguyen, T. Truong, Catal. Sci. Technol. 7 (2017) 3453–3458.
[10] I. Ahmed, B.N. Bhadra, H.J. Lee, S.H. Jhung, Catal. Today 301 (2018) 90–97.
[11] D.K. Yoo, H.J. An, N.A. Khan, G.T. Hwang, S.H. Jhung, Chem. Eng. J. 352 (2018) 71–78.
[12] H.J. An, B.N. Bhadra, N.A. Khan, S.H. Jhung, Chem. Eng. J. 343 (2018) 447–454.
[13] B.N. Bhadra, S.H. Jhung, Microporous Mesoporous Mater. 270 (2018) 102–108.
[14] N.A. Khan, D.K. Yoo, S.H. Jhung, ACS Appl. Mater. Interfaces 10 (2018) 35639–35646.
[15] T. Van Tran, D.T.C. Nguyen, H.T.N. Le, T.T.K. Tu, N.D. Le, K.T. Lim, L.G. Bach, T.D. Nguyen, J. Environ. Chem. Eng. (2019) 102881.
[16] M. Ma, A. Bétard, I. Weber, N.S. Al-Hokbany, R.A. Fischer, N. Metzler-Nolte, Cryst. Growth Des. 13 (2013) 2286–2291.
[17] T. Van Tran, D.T.C. Nguyen, H.T.N. Le, L.G. Bach, D.-V.N. Vo, S.S. Hong, T.-Q.T. Phan, T.D. Nguyen, Nanomaterials 9 (2019) 237.
[18] N. Liédana, P. Lozano, A. Galve, C. Téllez, J. Coronas, J. Mater. Chem. B. 2 (2014) 1144–1151.
[19] T. Van Tran, V. Dai Cao, V. Huu Nguyen, B.N. Hoang, D.-V.N. Vo, T.D. Nguyen, L. Giang Bach, J. Environ. Chem. Eng. (2019) 102902.
[20] P.S. Kumar, S. Ramalingam, C. Senthamarai, M. Niranjanaa, P. Vijayalakshmi, S. Sivanesan, Desalination 261 (2010) 52–60.
[21] S. Kaur, S. Rani, R.K. Mahajan, M. Asif, V.K. Gupta, J. Ind. Eng. Chem. 22 (2015) 19–27.
[22] S. Bauer, C. Serre, T. Devic, P. Horcajada, G. Férey, N. Stock, Inorg. Chem. 9 (2008) 7568–7576.
[23] D. Xie, Y. Ma, Y. Gu, H. Zhou, H. Zhang, G. Wang, Y. Zhang, H. Zhao, J. Mater. Chem. A. 5 (2017) 23794–23804.
[24] M.-H. Pham, G.-T. Vuong, A.-T. Vu, T.-O. Do, Langmuir 27 (2011) 15261–15267.
[25] X. Zhang, Y. Li, G. Li, C. Huh, RSC Adv. 5 (2015) 4984–4992.
[26] J. Wu, H. Gao, S. Yao, L. Chen, Y. Gao, H. Zhang, Separ. Purif. Technol. 147 (2015) 179–185.
[27] S. Cheng, L. Zhang, H. Xia, J. Peng, J. Shu, C. Li, RSC Adv. 6 (2016) 78936–78946.
[28] X. Peng, F. Hu, J. Huang, Y. Wang, H. Dai, Z. Liu, Microporous Mesoporous Mater. 228 (2016) 196–206.
[29] T. Van Tran, D.T.C. Nguyen, H.T.N. Le, O.T.K. Nguyen, V.H. Nguyen, T.T. Nguyen, L.G. Bach, T.D. Nguyen, R. Soc. Open Sci. 6 (2019) 190058.
[30] M. Muttakin, S. Mitra, K. Thu, K. Ito, B.B. Saha, Int. J. Heat Mass Transf. 122 (2018) 795–805.
[31] S.Z. Abidin, I.S. Mohamad, A.Y.B. Hashim, N. Abdullah, Proc. Mech. Eng. Res. Day. 2016 (2016) 127–128.
[32] J. He, Y. Zhang, X. Zhang, Y. Huang, Sci. Rep. 8 (2018) 1–8.
[33] S. Teixeira, C. Delerue-Matos, L. Santos, Sci. Total Environ. 646 (2019) 168–176.
[34] M.E. Roca Jalil, M. Baschini, K. Sapag, Appl. Clay Sci. 114 (2015) 69–76.
[35] K. Luo, Y. Pang, Q. Yang, D. Wang, X. Li, L. Wang, M. Lei, J. Liu, Chemosphere 231 (2019) 495–501.
[36] D.A. Palacio, B.L. Rivas, B.F. Urbano, Chem. Eng. J. 351 (2018) 85–93.
[37] H.N. Tran, S.-J. You, H.-P. Chao, Korean J. Chem. Eng. 34 (2017) 1708–1720.
[38] H. Li, W. Wu, X. Hao, S. Wang, M. You, X. Han, Q. Zhao, B. Xing, Environ. Pollut. 243 (2018) 206–217.
[39] B.H. Hameed, A.A. Rahman, J. Hazard Mater. 160 (2008) 576–581.
[40] T. Van Tran, D.T.C. Nguyen, H.T.N. Le, C.D. Duong, L.G. Bach, H.-T.T. Nguyen, T.D. Nguyen, Chemosphere 227 (2019) 455–461.
[41] C. Saucier, M.A. Adebayo, J. Hazard Mater. 289 (2015) 18–27.
[42] J.S. Piccin, T.R.S. Cadaval, L.A.A. de Pinto, G.L. Dotto, in: Adsorpt. Process. Water Treat. Purif., Springer, 2017, pp. 19–51.
[43] L.B. Escudero, E. Agostini, G.L. Dotto, Chem. Eng. Commun. 205 (2018) 122–133.
[44] S. Li, X. Zhang, Y. Huang, J. Hazard Mater. 321 (2017) 711–719.
[45] H. Mao, S. Wang, J.-Y. Lin, Z. Wang, J. Ren, J. Environ. Sci. 49 (2016) 179–188.
[46] T. Van Tran, D.T.C. Nguyen, H.-T.T. Nguyen, S. Nanda, D.-V.N. Vo, S.T. Do, T. Van Nguyen, T.A.D. Thi, L.G. Bach, T.D. Nguyen, Environ. Sci. Pollut. Res. (2019) 1–21.
[47] W. Li, C. Guangcai, L. Chen, Z. Jianfeng, S. Kathryn, Environ. Prog. Sustain. Energy 36 (2017) 1108–1115, https://doi.org/10.1002/ep.12579.
[48] Ş.S. Bayazit, S.T. Danalıoğlu, M. Abdel Salam, Ö. Kerkez Kuyumcu, Environ. Sci. Pollut. Res. 24 (2017) 25452–25461.
[49] S. Shi, Y. Fan, Y. Huang, Ind. Eng. Chem. Res. 52 (2013) 2604–2612.
[50] C.-J. Wang, Z. Li, W.-T. Jiang, Appl. Clay Sci. 53 (2011) 723–728.
[51] Y. Wu, Y. Tang, L. Li, P. Liu, X. Li, W. Chen, Y. Xue, Front. Chem. 6 (2018) 17.
[52] S.T. Danalıoğlu, Ş.S. Bayazit, Ö. Kerkez Kuyumcu, M.A. Salam, J. Mol. Liq. 240 (2017) 589–596.
[53] T. Van Tran, D.T.C. Nguyen, H.T.N. Le, L.G. Bach, D.-V.N. Vo, T.-U.T. Dao, K.T. Lim, T.D. Nguyen, J. Environ. Chem. Eng. 7 (2019) 103356.
[54] M. Sarker, J.Y. Song, A.R. Jeong, K.S. Min, S.H. Jhung, J. Hazard Mater. 344 (2018) 593–601.
[55] T. Van Tran, D.T.C. Nguyen, H.T.N. Le, L.G. Bach, D.-V.N. Vo, K.T. Lim, L.X. Nong, T.D. Nguyen, Molecules 24 (2019) 1887.